


## Article

# Analysis and Verification on Energy Consumption of the Quadruped Robot with Passive Compliant Hydraulic Servo Actuator

Zisen Hua <sup>1</sup>, Xuewen Rong <sup>1,\*</sup> , Yibin Li <sup>1</sup>, Hui Chai <sup>1</sup>, Bin Li <sup>2</sup>  and Shuaishuai Zhang <sup>3</sup>

<sup>1</sup> School of Control Science and Engineering, Center for robotics, Shandong University, Jinan 250061, Shandong, China; zmp3800@126.com (Z.H.); liyb@sdu.edu.cn (Y.L.); ch2200@sina.com (H.C.)

<sup>2</sup> School of Mathematics and Statistics, Qilu University of Technology (Shandong Academy of Sciences), Jinan 250353, Shandong, China; ribbonlee@126.com

<sup>3</sup> Department of Electrical Engineering and Information Technology, Shandong University of Science & Technology, Jinan 250031, Shandong, China; zhangshuaisdu@163.com

\* Correspondence: rongxw@sdu.edu.cn; Tel.: +86-0531-88392827

Received: 29 November 2019; Accepted: 26 December 2019; Published: 2 January 2020



**Abstract:** The hydraulic servo actuator with passive compliance (HPCA) is designed for hydraulically-driven quadruped robots. It is characterized by an accumulator that connects to the piston chamber of the hydraulic cylinder to buffer impact forces between a robot's feet and the ground. This paper studies the energy efficiency of this actuator in the dynamic locomotion of a quadruped robot. Different from the traditional methods of storing potentially recyclable energy using accumulators, the energy-saving principle of HPCA is to utilize the pressure-transition characteristics of the asymmetric hydraulic cylinder with control of the symmetrical valve. The accumulator can store and release oil during the switching of the transition point in each gait cycle of the robot, thereby improving the energy efficiency of the actuator. The influence of the initial inflation pressure and working volume of the accumulator on the energy efficiency of the HPCA is studied by simulation and physical experiments. The results show that the HPCA has a higher energy efficiency that is independent of the physical parameters of the accumulator.

**Keywords:** hydraulic servo actuator; accumulator; quadruped robot; trotting gait; energy efficiency

## 1. Introduction

Legged robots are receiving increased attention as the most prominent mobile robot technology for almost all terrain adaptations [1,2]. With the development of driving and sensing technology and the application of novel stabilization-control algorithms, stabilized locomotion and anti-disturbance capability become even more prominent, such as Bigdog [3,4] walking on ice and the back flips of Atlas [5]. However, compared to humans and animals, the energy efficiency of these robots remains relatively low [6].

The more general methods for improving the energy efficiency of legged robots can be divided into three classes: employment of structures or actuators with elastic or flexible components, passive locomotion, and motion optimization. For the first strategies, elastic or flexible elements, such as mechanical springs and rubber bands, are always connected to the limb structure to form passive joints, such as in HYQ designed by Claudio Semini et al. [7], and Cheetah, designed by Simon Rutishauser et al. [8]. Thus, the gravitational potential energy of the robot can be converted to elastic potential energy and released as the body moves forward. Elastic components can also be connected in series between the output of the actuator and the load to form a series elastic actuator [9,10] or a variable stiffness actuator [11,12]. These kinds of actuators not only can obtain the precise output force by

controlling the deformation of the elastomer but can improve energy efficiency through its rhythmic energy storage and discharge. The famous quadruped robot ANYmal is a successful application of this [13,14]. However, the limitation of the stiffness and complexity of the structure with the above methods make the structural design more complicated and reduce the adaptability of the robot to complex terrain.

Compared to the above strategies, passive locomotion seems to be the easiest way to improve energy efficiency. The three-dimensional passive walking robot designed by Cornell University [15] and inspired by McGeer [16] is representative. Not only can it walk stably on a slope, but it can achieve stable locomotion on a plane using motors and elastic mechanical springs in the ankle joint [17]. Unfortunately, such robots are developed for high energy efficiency and cannot be applied in practice. The most common method of motion optimization is to reduce the swing amplitude of the joint by optimizing the foot trajectory [18], which has obvious limitations for legged robots used in complex and unknown environments.

With its excellent power-to-weight ratio, high robustness, and high bandwidth, hydraulic actuation is used in many successful legged robots, such as Bigdog and LS3. With the development of high performance hydraulic components, highly efficient hydraulic servo systems have developed rapidly and are used in many fields, such as the load-sensing servo systems, pump/motor-controlled servo systems [19], and independent metering systems [20,21]. However, such systems are not suitable for legged robots. On the one hand, they are too complicated, and hydraulic components that can be applied to legged robots are relatively rare, while on the other hand, the performance of most of them is severely constrained by loads and the trajectory of the actuator, etc. The valve-controlled system [22] is still widely used on legged robots. It can provide good motion performance but cannot achieve its energy-saving potential. The energy efficiency can be significantly improved by using an ultra-low leakage valve or asymmetric spool servo valve [23], but such products with fast response and high control bandwidth are not only scarce but expensive.

The hydraulic servo actuator with passive compliance (HPCA) [24] was designed to improve the response of the actuator to impact forces between a robot's feet and the ground. The micro-hydraulic accumulator is connected to the piston chamber of the actuator, and its performance is also improved by various oil circuits and control valves. However, there is no relevant literature on the energy efficiency of the HPCA during quadruped robot movement. This paper comprehensively analyzes the actuator trajectory of a quadruped robot in the trotting gait and the dynamic/static pressure characteristics of the HPCA, and it clarifies that the main incentive for the improvement of energy efficiency is the pressure transition caused by the piston movement reversing that matches with the trajectory. Furthermore through motion simulation of a quadruped robot and a physical experiment based on a single-leg platform, the effectiveness of HPCA for the improvement of the energy efficiency of a quadruped robot is verified, and the influence of different parameters of the accumulator on the energy efficiency of the HPCA is clarified. We believe this is the first time that the accumulator has been combined with the pressure-transition characteristics of the actuator to improve energy efficiency.

The rest of this article is structured as follows. Section 2 describes the HPCA. Section 3 analyzes the actuator trajectory in a robot's trotting gait and chamber pressure characteristics of the HPCA and further deduces the energy-saving law of the actuator. In Section 4, simulation results are presented. Section 5 illustrates the experimental results. Section 6 relates our conclusions.

## 2. Overview of HPCA

The HPCA is a further improvement to the actuator with the original structure used on hydraulic quadruped robots, as shown in Figure 1. As can be seen from Figure 1A, the original hydraulic servo actuator used on the quadruped robot is characterized by integrating a servo valve, force sensor, and displacement sensor into the hydraulic cylinder. Compared to the original structure, the HPCA shown in Figure 1B is equipped with not only the hydraulic servo valve and various sensors but a micro accumulator and filling-oil circuit. The accumulator changes the stiffness characteristics of the actuator

to reduce the pressure fluctuations in the working chamber. The filling-oil circuit controlled by the check valve can effectively prevent cavitation. Therefore, the vacancy caused by the retraction of the piston can be quickly filled by the oil from the return oil circuit through the check valve. This early engineering verification product does not employ a highly-integrated design nor advanced manufacturing technology, and control valves are connected with oil circuits inside the ordinary hydraulic cylinder via two oil blocks. The mass of the original actuator is 2.76 kg, and the mass of the HPCA increases by 0.92 kg.

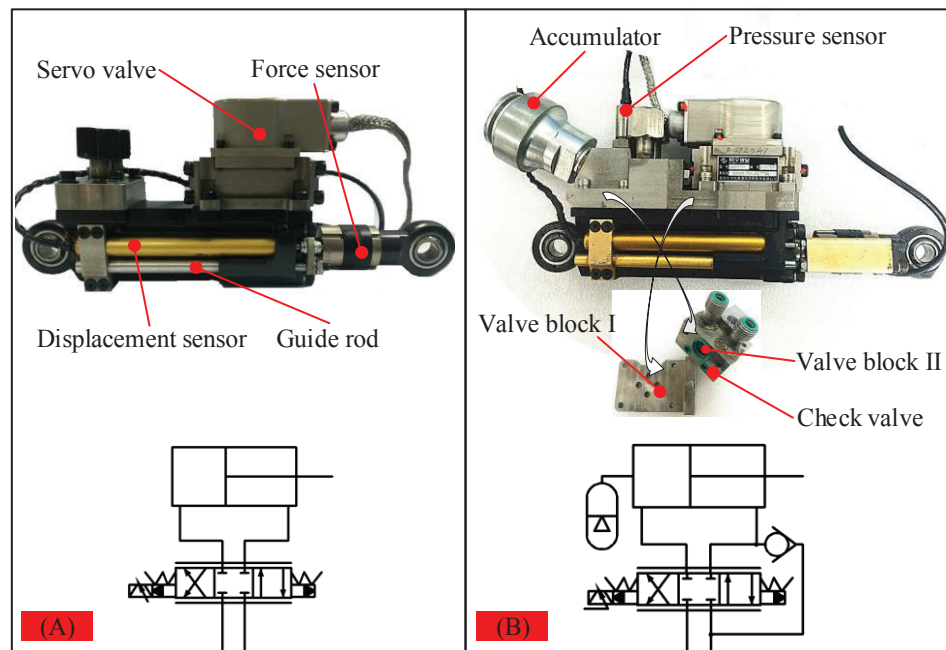


**Figure 1.** Hydraulic servo actuator. (A) Actuator with original structure and corresponding hydraulic principle; (B) hydraulic servo actuator with passive compliance (HPCA) and corresponding hydraulic principle.

### 3. Energy-Saving Principle of HPCA

#### 3.1. Motion Description of SCalf II

SCalf II is the hydraulically actuated quadruped robot designed by Shandong University in 2012 for orientation in rough terrains [25]. As can be seen from Figure 2A, 12 degree-of-freedom (DOF) topology is adopted because it cannot only provide a sufficient range of motion but can reduce the complexity of mechanical structures and control algorithms. Each leg (Figure 2B) includes three rotating joints: two pitch joints used for flexion and extension (hip F/E and Knee F/E) at the knee and hip, and a roll joint used for adduction and abduction at the hip (hip A/A). Under normal conditions, hip F/E and knee F/E are the main contributors to foot trajectory implementation, and hip A/A only participates in movement during attitude adjustment of the robot torso. With better energy efficiency and stability, trotting [26] has become the most basic and most commonly used gait for quadruped robots, and a gait cycle can be decomposed to supporting and swing phases. The torso moves forward in the supporting phase, while the leg swings forward in the swing phase.

To have a smooth transition from the supporting phase to the swing phase and eliminate the fluctuation of the torso, the velocity of the robot along the x-axis should be constant during the whole gait period, and the velocity along the z-axis should be set to zero at the starting point, the ending point, and the highest point of the swing phase. Abrupt change points should not appear on the velocity and acceleration curves throughout the cyclic gait. In this paper, the foot trajectory with duty

factor  $\beta = 0.5$  (the fraction of a cycle time during which the leg is in the supporting phase) described in previous work [1,27] is used and can be expressed as:

$$\begin{cases} x_{fsw} = L(\frac{192t^5}{T^5} - \frac{240t^4}{T^4} + \frac{80t^3}{T^3} - \frac{t}{T}) \\ x_{fsu} = -\frac{Lt}{T} + L \\ z_{fsw} = H(\frac{256t^4}{T^4} - \frac{256t^3}{T^3} + \frac{64t^2}{T^2}) \\ z_{fsu} = 0, \end{cases} \quad (1)$$

where subscripts  $fsw$  and  $fsu$  indicate the swing phase and supporting phase, respectively, and  $L$ ,  $H$ , and  $T$  are, respectively, the length, height and cycle of the gait.

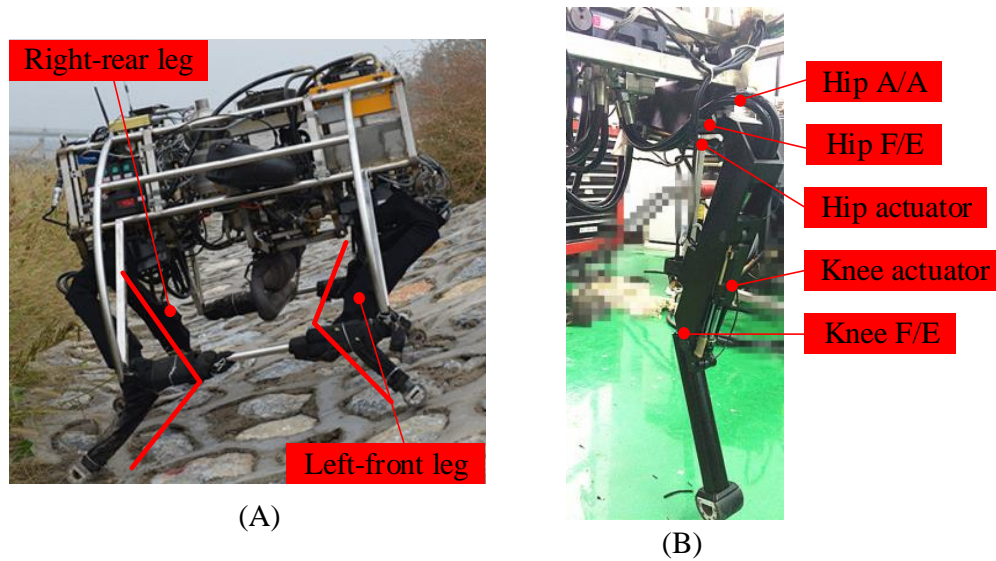


**Figure 2.** Hydraulically actuated quadruped robot SCalf II. (A) Picture of SCalf II; (B) leg structure used by SCalf II.

Taking the left-front and right-rear legs as examples, Figure 3 shows the foot trajectory and the motion curves of the actuators (hip F/E and knee F/E) calculated by leg kinematics [25]. The three displacement curves shown in Figure 3C use the initial points (the starting points of each gait cycle) shown in Figure 3B as starting points. The distances from points  $O_1$  to  $O$  and  $O_2$  to  $O$  are both 0.15 m. As can be seen from the curves, each actuator performs the same motion process in the swing phase, retracting first and then extending, while in the supporting phase, there is a big difference between the actuator trajectories at different positions, monotonous retraction or monotonous elongation.

Since the mass of the leg components is much lighter than that of the torso, the loads applied to the actuators in the swing phase are obviously smaller than that in the supporting phase. Unfortunately, the output force of the hydraulic actuator is generated by the pressure difference between the piston chamber and ring chamber, which is affected by the supply pressure. Thus, the inessential energy-loss is predominantly in the swing phase. Moreover, it can be seen from Figure 3B that, for the knee F/E, the direction of the torque exerted by the interaction force between the ground and foot on the rotating joint is not affected by the position of the initial points but not for the hip F/E. The same principle has always held by the direction of the actuator output forces. When the initial point is on the right side of  $O$  (e.g.,  $O_2$ ), the hip actuator mainly bear tension; otherwise, it is always subjected to compression. But, for the knee actuator, it always sustain compression.

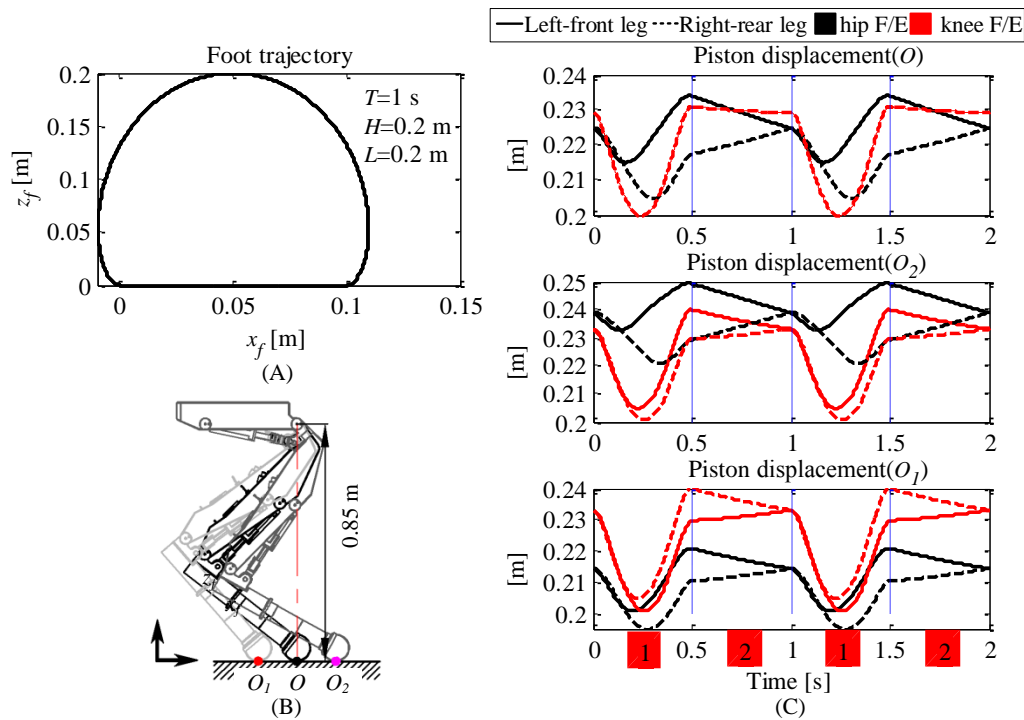


**Figure 3.** Foot trajectory and piston movement. (A) Foot trajectory; (B) initial points; (C) piston displacement. Numbers 1 and 2 represent the swing phase and supporting phase, respectively. F/E = flexion and extension.

### 3.2. Pressure Characteristics of HPCA

#### 3.2.1. Dynamic Pressure Characteristic

In Figure 4,  $P$ ,  $V$ ,  $A$ , and  $Q$  represent pressure, volume, area, and flow, respectively, and the subscripts  $pis$ ,  $r$ ,  $accu$ , and  $S$  denote the piston chamber, ring chamber, accumulator, and oil supply port, respectively. The area ratio  $\alpha$  can be described as  $A_r/A_{pis}$ .  $x_p$  is the respective positions of the piston and valve core.  $V_{g0}$  and  $P_{g0}$  represent the initial working volume and inflation pressure, respectively, of the accumulator. The output force and load force are indicated by  $f_h$  and  $f_l$ , respectively.  $Q_c$  represents the flow through the check valve.

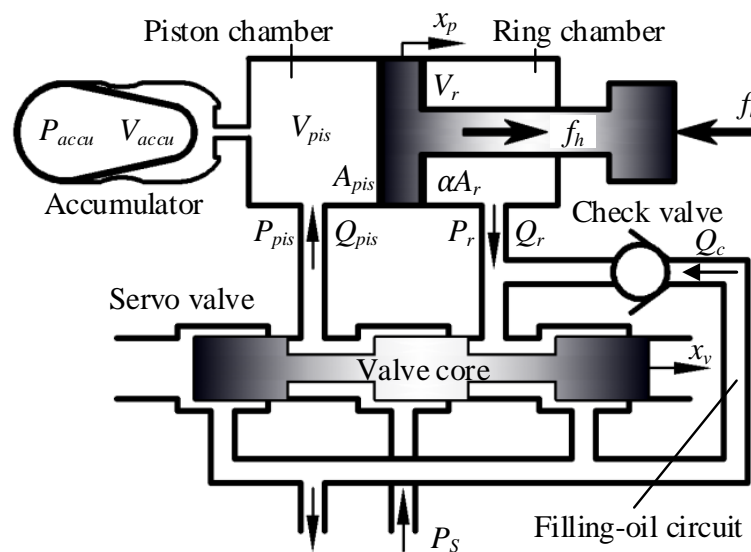


**Figure 4.** Definition of variables for hydraulic schematic diagram of HPCA.



For the actuator with the original structure (Figure 1A), regardless of the internal and external leakage, pressure dynamics in working chambers can be expressed as [27]:

$$\begin{cases} \dot{P}_{pis} &= \frac{(Q_{pis} - A_{pis}\dot{x}_p)\beta_e}{A_{pis}(x_{p0} + x_p)} \\ \dot{P}_r &= \frac{(Q_r + A_r\dot{x}_p)\beta_e}{A_r(x_{stroke} - x_{p0} - x_p)}, \end{cases} \quad (2)$$

where  $\beta_e$  is the effective bulk modulus of the system;  $x_{p0}$  is the initial position of the piston, and  $x_{stroke}$  is the total stroke of the hydraulic cylinder.

According to Boyle's law [28], the relationship between the working chamber of the accumulator and the inflation pressure can be expressed as:

$$P_{g0} \cdot V_{g0}^n = P_{accu} \cdot V_{accu}^n = CONST, \quad (3)$$

where  $n$  is determined by the working status of the accumulator. In the isothermal condition,  $n = 1$ ; in the adiabatic condition,  $n = 1.4$ .

Differentiating  $P_{accu}$  from Equation (3) gives:

$$\dot{P}_{accu} = \begin{cases} 0 & (P_{pis} \leq P_{g0}) \\ \frac{-nP_{g0}V_{g0}^n Q_{accu}}{V_{accu}^{n+1}} & (P_{pis} > P_{g0}) \end{cases}, \quad (4)$$

where  $Q_{accu}$  is the flow rate at the port of the accumulator.

For the HPCA, when the gasbag in the accumulator is compressed ( $P_{pis} > P_{g0}$ ), the conditions

$$\begin{cases} P_{pis} &= P_{accu} \\ \dot{P}_{pis} &= \dot{P}_{accu} \end{cases} \quad (5)$$

are satisfied and the pressure dynamics of the actuator can be described as:

$$\begin{cases} \dot{P}_{pis} &= \frac{nP_{g0}V_{g0}^n(Q_{pis} - A_{pis}\dot{x}_p)}{V_{accu}^{n+1}} \\ \dot{P}_r &= \frac{\beta_e(Q_r + A_r\dot{x}_p + Q_c)}{V_r}. \end{cases} \quad (6)$$

Figure 5 shows the relationship between the scale factors  $\beta_e/V_{pis}$  and  $nP_{g0}V_{g0}^n/V_{accu}^{n+1}$  that determine the rate change of the piston chamber pressure as described in Equations (2) and (6). The referenced data are shown in Table 1, among which the working volume of the accumulator  $V_{accu}$  is set to 25% of the initial working volume  $V_{g0}$  that is the minimum value allowed during normal use. Therefore, the scale factor of the HPCA can be regarded as the maximum value at each point. It can be seen from the curves that the addition of the accumulator greatly reduces the rate change of the chamber pressure, which is advantageous for reducing pressure fluctuations.

**Table 1.** Parameters of actuator.

Description	Symbol	Value	
piston diameter	\	0.025	m
piston rod diameter	\	0.012	m
piston stroke	$x_{stroke}$	0.072	m
initial working volume	$V_{g0}$	$1.3 \times 10^{-5}$	m <sup>3</sup>
bulk modulus	$\beta_e$	1400	Mpa
working volume	$V_{accu}$	$1.3 \times 10^{-5} \times 0.25$	m <sup>3</sup>

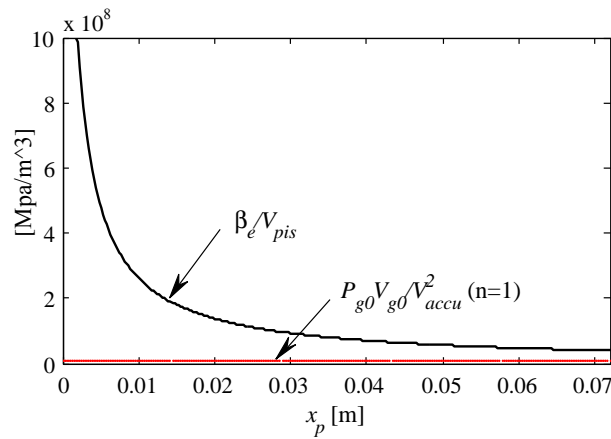


Figure 5. Parameter comparison.

### 3.2.2. Static Pressure Characteristic

For the asymmetric hydraulic cylinder with control of the symmetric servo valve shown in Figure 4, the force balance on the cylinder can be calculated as [29]:

$$A_{pis}P_{pis} - \alpha A_{pis}P_r = f_h = f_l. \quad (7)$$

Again, ignoring the leakage and oil compressibility, the following relationship will be satisfied according to the flow continuity equation :

$$\begin{cases} \frac{K\sqrt{P_S - P_{pis}} - Q_{accu}}{A_{pis}} = \frac{K\sqrt{P_r}}{\alpha A_{pis}} & \dot{x}_p > 0 \\ \frac{K\sqrt{P_{pis} + Q_{accu}}}{A_{pis}} = \frac{K\sqrt{P_S - P_r}}{\alpha A_{pis}} & \dot{x}_p < 0, \end{cases} \quad (8)$$

with

$$K = C_d x_v A, \quad (9)$$

where  $C_d$  and  $A$  are the flow coefficient and area gradient, respectively; the positive and negative of  $\dot{x}_p$  indicate the extension and retraction of the piston;  $Q_{accu}$  can be described as:

$$Q_{accu} = \frac{\dot{P}_{accu} P_{g0}^{1/n} V_{g0}}{n P_{accu}^{(n+1)/n}}. \quad (10)$$

Since the chamber pressures  $P_{pis}$  and  $P_r$  cannot be accurately solved by directly implementing Equation (8), only pressure characteristics at the moment of piston reversal are considered. Since the working volume of the accumulator  $V_{accu}$  cannot change during this extremely short time, the following relationships are still satisfied before and after the reversal:

$$\begin{cases} P_{accu}(t - \Delta t) = P_{accu}(t + \Delta t) \\ \dot{P}_{accu}(t - \Delta t \leq t \leq t + \Delta t) = 0, \end{cases} \quad (11)$$

where  $t$  is the moment of reversal, and  $\Delta t \rightarrow 0$ .

Then, Equation (8) can be rewritten as:

$$\begin{cases} \frac{K\sqrt{P_S - P_{pis}}}{A_{pis}} = \frac{K\sqrt{P_r}}{\alpha A_{pis}} & \dot{x}_p > 0 \\ \frac{K\varphi\sqrt{P_{pis}}}{A_{pis}} = \frac{K\sqrt{P_S - P_r}}{\alpha A_{pis}} & \dot{x}_p < 0 \end{cases} \quad (12)$$

Taking into account Equations (7) and (12), the pressure in the working chambers can be described as:

For  $\dot{x}_p > 0$ ,

$$\begin{cases} P_{pis} &= \frac{\alpha^3 A_{pis} P_S + f_l}{A_{pis}(1 + \alpha^3)} \\ P_r &= \frac{\alpha^2 (A_{pis} P_S - f_l)}{A_{pis}(1 + \alpha^3)}. \end{cases} \quad (13)$$

For  $\dot{x}_p < 0$ ,

$$\begin{cases} P_{pis} &= \frac{\alpha A_{pis} P_S + f_l}{A_{pis}(1 + \alpha^3)} \\ P_r &= \frac{A_{pis} P_S - \alpha^2 f_l}{A_{pis}(1 + \alpha^3)}. \end{cases} \quad (14)$$

For asymmetric hydraulic cylinders,  $\alpha$  is less than 1, and the following rules will be met:

$$\begin{cases} P_{pis}(\dot{x}_p > 0) &< P_{pis}(\dot{x}_p < 0) \\ P_r(\dot{x}_p > 0) &< P_r(\dot{x}_p < 0). \end{cases} \quad (15)$$

This means that a pressure transition will be generated in the working chamber of the HPCA due to the piston reversal. When the piston changes from extracting to retracting, both the chamber pressures ( $P_{pis}$  and  $P_r$ ) increase, and vice versa.

### 3.2.3. Working Principle of Accumulator Used on HPCA

In traditional energy-regeneration hydraulic systems [30,31], the gravitational potential energy or kinetic energy is converted to pressure energy by the hydraulic pump/motor, and it is stored in the accumulator. However, a quadruped robot keeps moving forward through the rhythmic swing of the limbs according to the planned trajectory, and the motion and load characteristics cause the robot to have no potential gravitational potential or kinetic energy that can be utilized. Therefore, as can be seen from Figure 6, unlike the traditional use of the accumulator to save energy, the working principle of the accumulator used on the HPCA combines the pressure characteristics of the HPCA with the trajectory of the piston under the planned gait, which can be detailed and compared as follows.

- (1) In the swing phase, all actuators conform to the law that varies first retraction and then extension, and the pressure in the piston chamber tends to be less. For the actuator with original structure, the flows required for the further extension of the piston and compensation for the pressure drop are all provided by the servo valve. But, for the HPCA, part of the required flows mentioned above can be supplied by the accumulator. Thus, the supply flow from the power source needed by the system with HPCA is less than that with the original actuator in this process.
- (2) In the supporting phase, a rather large difference in the piston trajectory exists between the actuators that drive different joints. For the same actuator, the different initial point will also cause differences. If the piston is in the process of retraction (Figure 6A), the change in direction from elongation to shortening causes the pressure in the piston chamber to be greater. For the actuator with original structure, the raised backward pressure can result in increased pressure loss in the throttle of the servo valve, so the inessential energy-loss will also increase. For the HPCA, the pressure increase due to the piston reversal is slowed down by the accumulator (as explained in Equations (2) and (6)) on the one hand, on the other hand, the oil that flows out from the piston chamber can be partially stored in the accumulator and is supplied to the next gait cycle. When the piston is in the process of extension (Figure 6B), the flow required by this process is only provided by the servo valve. The abrupt point of the chamber pressure occurs when the trajectory transitions from the support phase to the swing phase of the next cycle, and then the law described above is carried out.



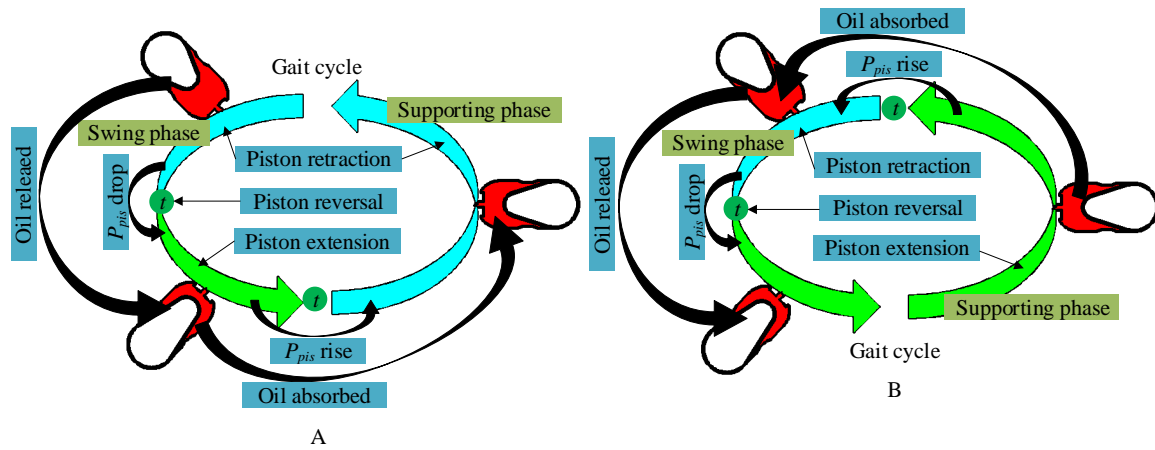


**Figure 6.** Working principle of accumulator. (A) situation number one; (B) situation number two.

From the above analysis, it can be seen that the oil storage and offloading process of the accumulator due to the piston reversal always occur in each gait cycle, no matter which rotating joint the HPCA drives nor where the initial point is located. Therefore, the HPCA has lower energy consumption than the original actuator.

#### 4. Simulation and Analysis

##### 4.1. System Modeling

To test the energy saving of the actuator and find some rules for robot design, a simulation was carried out in the advanced modeling environment for performing simulation of engineering systems (AMESim) [32]. The mechatronics-hydraulics-integrated model of the SCalf II is shown in Figure 7. Since the keystone of this paper is the energy efficiency of the actuator, the attitude adjustment of the robot is not considered, and the Planar Mechanical Library (the components marked with blue) can be used to build the mechanical system. The related structural and physical parameters were obtained by CAD software. Since the actuators are almost non-rotating over the entire stroke length, the influence of the actuators on the leg dynamics can be ignored, and the mass is dispersed to the connected components on both sides. To get a concise model, the hydraulic systems and controller of each leg are created by the supercomponents marked by black and red, respectively. The actuators and other hydraulic related components (components marked by pink and light green) can be built by the corresponding module in Hydraulic Library. The relevant components of the controllers can be obtained from the Signal Control Library. To simplify the problem and facilitate theoretical analysis, this study only discusses the situation when the initial point is at position O shown in Figure 3.

In the simulation, the compliant control method based on the virtual model (VMC) [33] was used. The desired joint torque can be established as:

$$\begin{bmatrix} \tau_{hip} \\ \tau_{knee} \end{bmatrix} = J^T V_f + PD(\theta_{hip}, \theta_{knee}) \quad (16)$$

with

$$V_f = \begin{bmatrix} k_x \Delta x_f + b_x \Delta \dot{x}_f \\ k_z \Delta z_f + b_z \Delta \dot{z}_f \end{bmatrix} + \begin{bmatrix} 0 \\ Mg \end{bmatrix} \quad (17)$$

and

$$PD(\theta) = \begin{bmatrix} K_p \Delta \theta_{hip} + K_d \Delta \dot{\theta}_{hip} \\ K_p \Delta \theta_{knee} + K_d \Delta \dot{\theta}_{knee} \end{bmatrix} \quad (18)$$

where  $\tau$  and  $\theta$  are the torque and joint angle, respectively, and the subscripts *hip* and *knee* indicate the corresponding positions;  $k$  and  $b$ , respectively, represent the virtual stiffness and virtual damping,

and the subscripts  $x$  and  $z$  denote the corresponding directions;  $x_f$  and  $\dot{x}_f$ , respectively, represent the displacement and velocity of the reference point on the robot's foot along the  $x$ -axis, and the difference between the actual and target positions is  $\Delta$ . The annotations follow the same rules in other directions;  $Mg$  is the gravity compensation, which only works during contact between the foot and the ground;  $K_p$  and  $K_d$  are the gain coefficients of the PID controller.

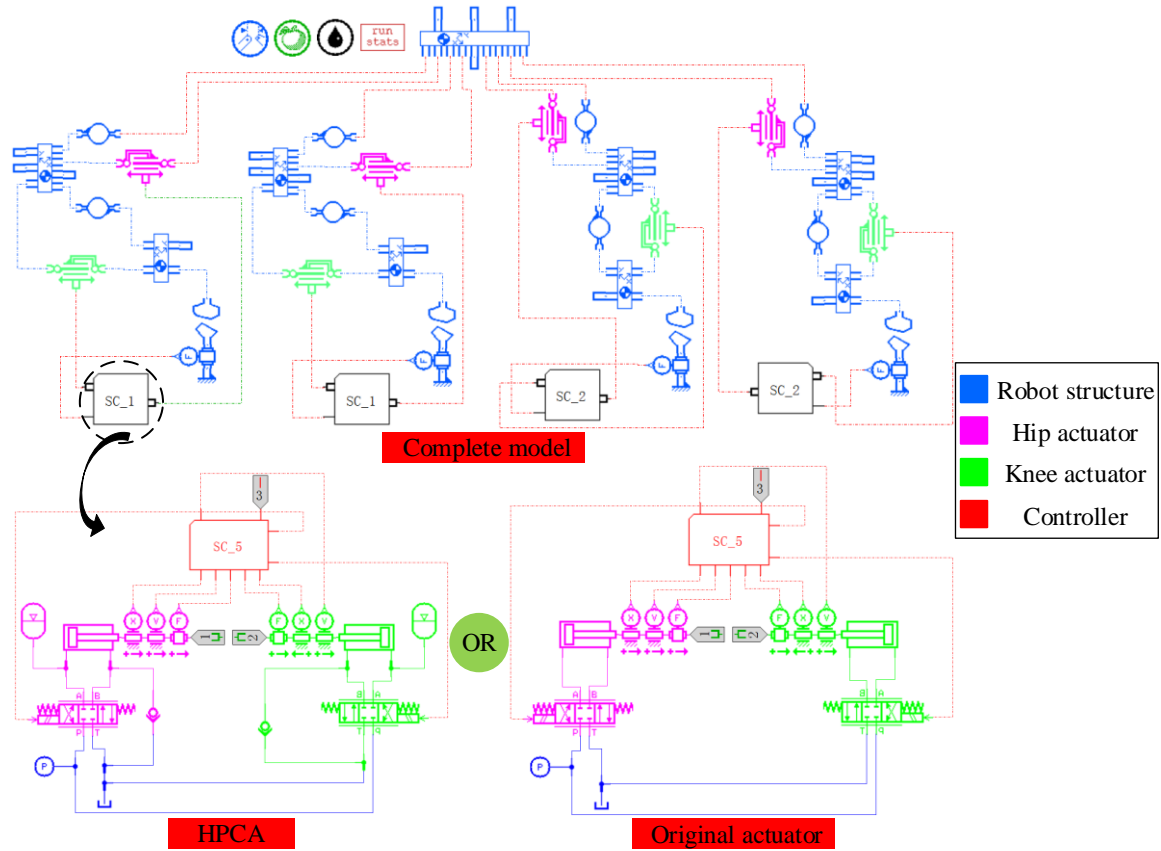


Figure 7. Model built in AMESim.

The overall control architecture is shown in Figure 8. The actual foot positions ( $x_f$  and  $z_f$ ) and joint angles are calculated through the leg and joint kinematics based on the piston positions  $x_p$ . The desired joint angles are obtained through the joint kinematics based on the foot trajectory.

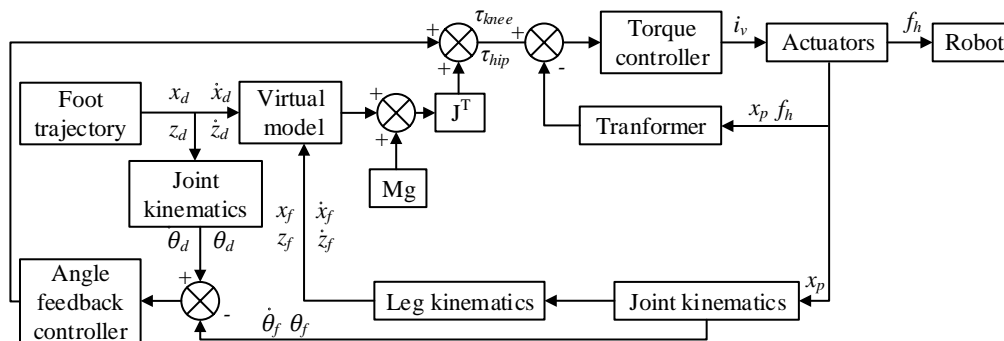


Figure 8. Control architecture of leg prototype.

#### 4.2. Simulation Setup

The fifth-order foot trajectory described in Section 3.1 is used in the simulation. The whole simulation course can be divided into two experimental groups, depending on the initial inflation pressure and the working volume of the actuator. The settings and differences are as follows.

- (1) In group 1, the initial inflation pressure of the accumulator  $P_{g0}$  was set to 2, 4, and 6 Mpa. The working volume of the actuator  $V_{g0}$  is constant ( $1.3 \times 10^{-5} \text{ m}^3$ ).
- (2) Different from group 1, the initial inflation pressure of the actuator was constant (6 Mpa) in group 2, and the working volumes were set to  $2 \times 10^{-5}$ ,  $4 \times 10^{-5}$ , and  $6 \times 10^{-5} \text{ m}^3$ .

The actuator with the original structure was also simulated and used for comparison. The parameters of the cylinder are shown in Table 1, and the rest of the parameters are shown in Table 2.

**Table 2.** Parameters of simulation.

Description	Symbol	Value
input pressure	$P_S$	20 Mpa
torso mass		110 kg
gait length	$L$	0.236 m
gait height	$H$	0.1 m
gait cycle	$T$	1 s
stiffness in $x$ -axis	$k_x$	5000 N/m
stiffness in $z$ -axis	$k_z$	8000 N/m
damping in $x$ -axis	$b_x$	10 N/m/s
damping in $z$ -axis	$b_z$	15 N/m/s

#### 4.3. Simulation Results

Because with better representative, the simulation results of the hip actuator (hip F/E) at the left-rear and right-front legs are only shown in Figure 9. The desired trajectories ( $x_p$  in legend) of the actuators magnified by a corresponding multiple are used as a reference in some pictures. It can be seen from the results that, for the hip actuator at the left-front leg, the first abrupt point of the piston chamber pressure ( $P_{pis}$ ) always occurs in 0.15 s during the swing phase, and the second appears at the transition from the swing phase to the supporting phase, while for the actuator at the right-rear leg, the first abrupt point of the piston chamber pressure ( $P_{pis}$ ) always occurs in 0.35 s during the swing phase, and the second abrupt point appears at the transition from the supporting phase to the swing phase of the next cycle.

As can be seen from the flow curves ( $Q_{accu}$ ), the positive parts indicate that the accumulator, as a flow source, always supplies fluid for the piston extension, while the negative parts indicate that the accumulator, as an energy-storage unit, has been absorbing the oil released by the piston retraction. The energy consumption curves shown in the Figure 9 can be obtained by integrating the power ( $Q_S \times P_S$ ). The energy consumption values at each point of the piston reversal are shown in Tables 3 and 4. It can be seen that, for the actuator at left-front leg, the energy consumption of the original actuator increases by 148.6 J, 119 J, 148 J, and 85 J between the reversal points. But, for the HPCA, such data is around 122 J, 119 J, 122 J, and 84 J, respectively. This is consistent with the law described in Section 3.2.3, which indicates that the process of the piston from shortening to elongation can release energy. For the actuator at rear-right leg, such values are 149 J, 130 J, and 149 J for the original actuator and are around 134 J, 128 J, and 134 J for the HPCA. This is also consistent with the law described in Section 3.2.3. It is worth adding that the energy released is caused by the pressure transition of the piston from extension to retraction.

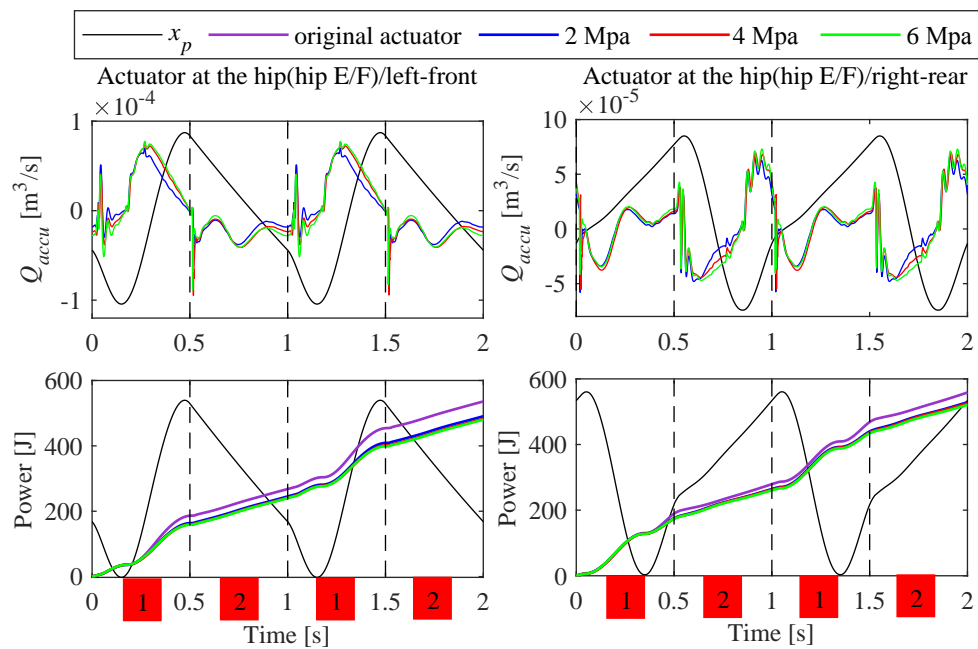


**Figure 9.** Performance of HPCA with different initial inflation pressure of the accumulator. Numbers 1 and 2 represent the swing and supporting phase, respectively.

**Table 3.** Energy consumption of the hip actuator at left-front leg.

Description	First (0.15 s)	Second (0.47 s)	Third (1.15 s)	Fourth (1.47 s)	Total (2 s)
original actuator	34.04 J	182.1 J	302 J	450 J	535.8 J
2 Mpa	34.5 J	160.4 J	279.7 J	405.7 J	490.5 J
4 Mpa	34.7 J	156.7 J	275.9 J	398 J	482.6 J
6 Mpa	34.7 J	155.8 J	274.8 J	395.9 J	480.3 J

**Table 4.** Energy consumption of the hip actuator at rear-front leg.

Description	First (0.35 s)	Second (1 s)	Third (1.35 s)	Total (2 s)
original actuator	130.2 J	279.2 J	409.4 J	558.4 J
2 Mpa	128 J	264.2 J	392.5 J	528.8 J
4 Mpa	128 J	262.7 J	390.7 J	525.4 J
6 Mpa	128 J	260.4 J	387.9 J	520.8 J

The simulation results of group 2 are displayed in Figure 10 in the same way as for group 1, and the incremental energy consumption between the reversal point is shown in Tables 5 and 6. It can be seen that the influence of the working volume change of the accumulator on the energy efficiency of the actuator is the same as caused by the change of the initial inflation pressure detailed above, and the increase in the working volume of the accumulator does not significantly improve the energy efficiency of the HPCA during the reversal of the piston from contraction to extension. This is also consistent with the law described in Section 3.2.3.

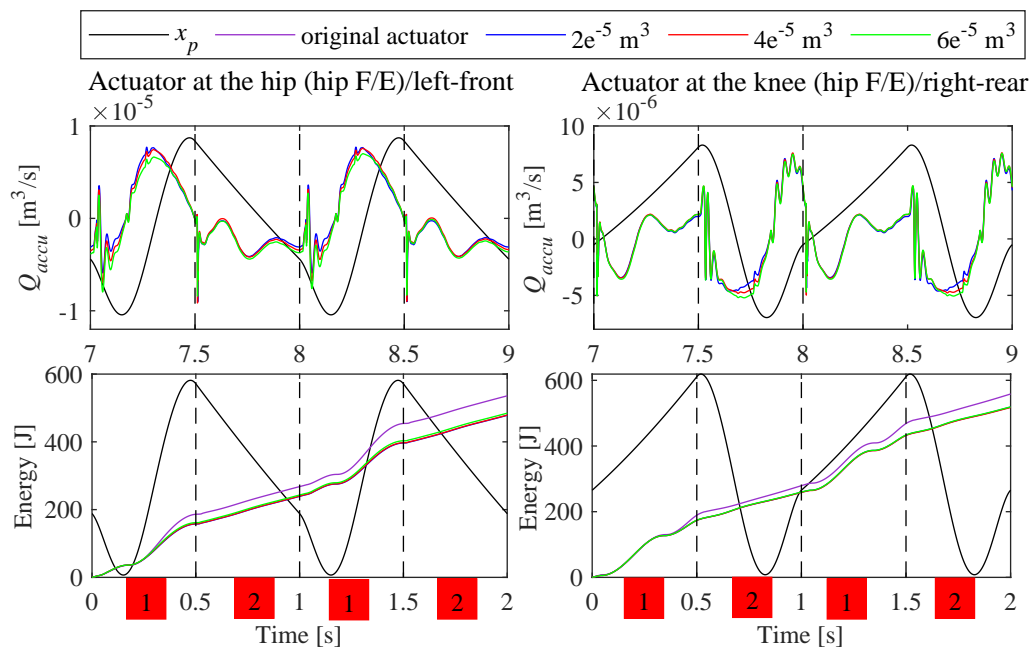


**Figure 10.** Performance of HPCA with different working volume of accumulator.

**Table 5.** Energy consumption of the hip actuator at left-front leg.

Description	$\Delta J_{1,2}$	$\Delta J_{2,3}$	$\Delta J_{3,4}$	$\Delta J_{total,4}$
original actuator	147 J	119 J	148 J	84.5 J
$2 \times 10^{-5} \text{ m}^3$	120.8 J	119 J	119.4 J	84.6 J
$4 \times 10^{-5} \text{ m}^3$	120.6 J	119 J	120 J	84.8 J
$6 \times 10^{-5} \text{ m}^3$	121.5 J	119.1 J	119.6 J	85.1 J

**Table 6.** Energy consumption of the hip actuator at rear-right leg.

Description	$\Delta J_{1,2}$	$\Delta J_{2,3}$	$\Delta J_{total,3}$
original actuator	149	130.2	149
$2 \times 10^{-5} \text{ m}^3$	132.5 J	125.8 J	133.6 J
$4 \times 10^{-5} \text{ m}^3$	132.7 J	125.8 J	133.6 J
$6 \times 10^{-5} \text{ m}^3$	132.3 J	126.1 J	133.9 J

The above results prove that the HPCA does not play a role in energy conservation in the supporting phase, and in the swing phase, the energy efficiency of the actuator is not greatly affected by the initial inflation pressure and working volume of the accumulator. The explanation for this phenomenon can be summarized as follows:

- (1) In the supporting phase, the piston chamber of the actuator at left-front leg is connected to the oil return circuit, and the flow required for the piston movement is mainly supplied by the servo valve. Thus, the energy supplied by the power source is the same whether it is the original actuator or the HPCA. But, for the actuator at rear-right leg, the piston is in the extension stage and sustains compression, and the ring chamber of the actuator is connected to the oil return circuit. Because of the unequal area of the piston, a large flow required causes the opening of the valve core to increase, and then there is a large pressure drop in the ring chamber (as shown in Figure 11). Therefore, a smaller pressure fluctuation in the piston chamber can be enough to adjust actuator output to balance the load.
- (2) In the swing phase, due to the small fluctuation of the loads, the pressure difference between the piston and ring chambers of the two actuators remains relatively stable, as can be seen from

Figure 11. Therefore, the oil supplied by the power source for the piston movement seldom flows into the accumulator. The steps to improve the energy efficiency by changing the inflation pressure and working volume of the HPCA will have little effect.

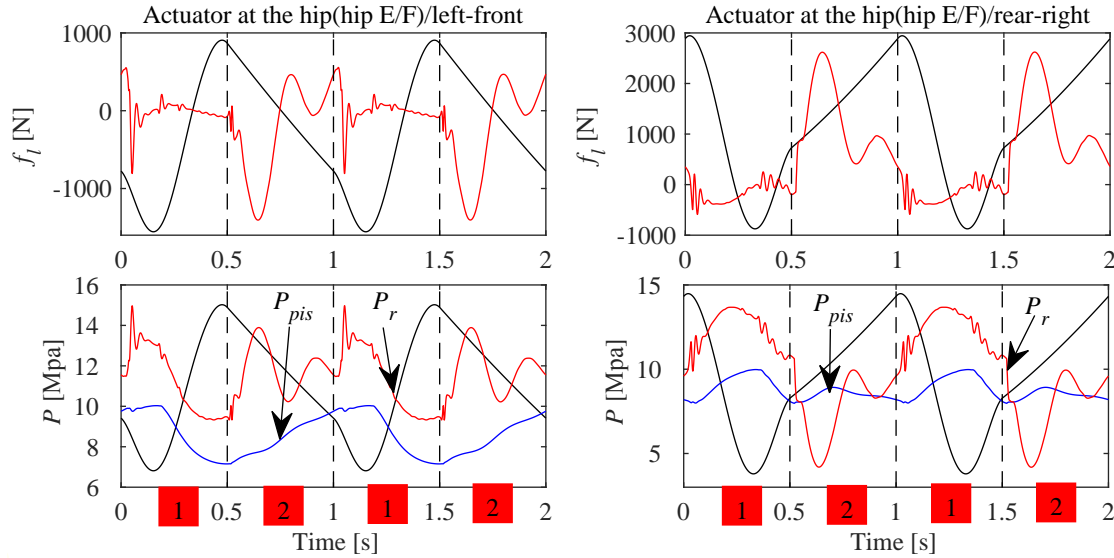


Figure 11. Chamber pressure and loads of hip actuators with the initial inflation pressure of 20 Bar.

## 5. Experimental Verification

### 5.1. Experimental Setup

Due to limitations of devices, it is currently not possible to test the HPCA on a robot platform. Therefore, a single-leg test bench was designed to verify the simulation results. As can be seen from Figure 12, the test bench is mainly composed of beam I and II connected by slider in horizontal direction. The slider in vertical direction is mounted on the beam II and connects to the counterweight, so that the counterweight can only move in the vertical direction along beam II. The counterweight and hip are connected by bolts so that the leg can only swing in the x-z plane relative to the counterweight. According to the experimental setting, the lateral movement of beam II is limited. The total mass of the leg prototype is 45.3 kg.

The experiment was divided into two groups with aims to test the energy efficiency characteristics of the HPCA with different loads and foot trajectories. In group 1, the leg prototype was mounted on the hanging bracket and could not touch the ground during the experiment. The foot trajectory described in Section 3.1 was used. In group 2, the foot remained in contact with the ground at all times and the initial standing height of the robot is set to 0.65 m. The sinusoidal signal with frequency of 1 Hz and amplitude of 0.05 m was used as the foot trajectory in the z-axis and the desired trajectory was set to zero along the x-axis. A large hydraulic station ensured a constant supply pressure for the experiment (200 bar).

A flow sensor cannot be installed between the accumulator and cylinder, so the flow data  $Q_{accu}$  can be calculated by Equation (10). The pressure in the piston chamber  $P_{accu}$  can be measured by the miniature pressure sensor (Model: TE/EB1UM- 00000P- 350BA) mounted on the actuator, and then the change of the pressure  $\dot{P}_{accu}$  can be obtained through deriving  $P_{accu}$ . The energy consumption of the leg prototype can be calculated as follows:

$$E = \int W_{hip} dt + \int W_{knee} dt \quad (19)$$



with

$$W_{hip}(W_{knee}) = \begin{cases} (A_{pis}\dot{x}_p - Q_{accu})P_S & (\dot{x}_p > 0) \\ A_r P_S |\dot{x}_p| & (\dot{x}_p < 0), \end{cases} \quad (20)$$

where the displacement of the piston  $x_p$  can be measured by the linear transducer (model: VISHAY/REC 38L 03C 502 B) mounted on the actuator, and then the velocity  $\dot{x}_p$  can be obtained through deriving  $x_p$ .

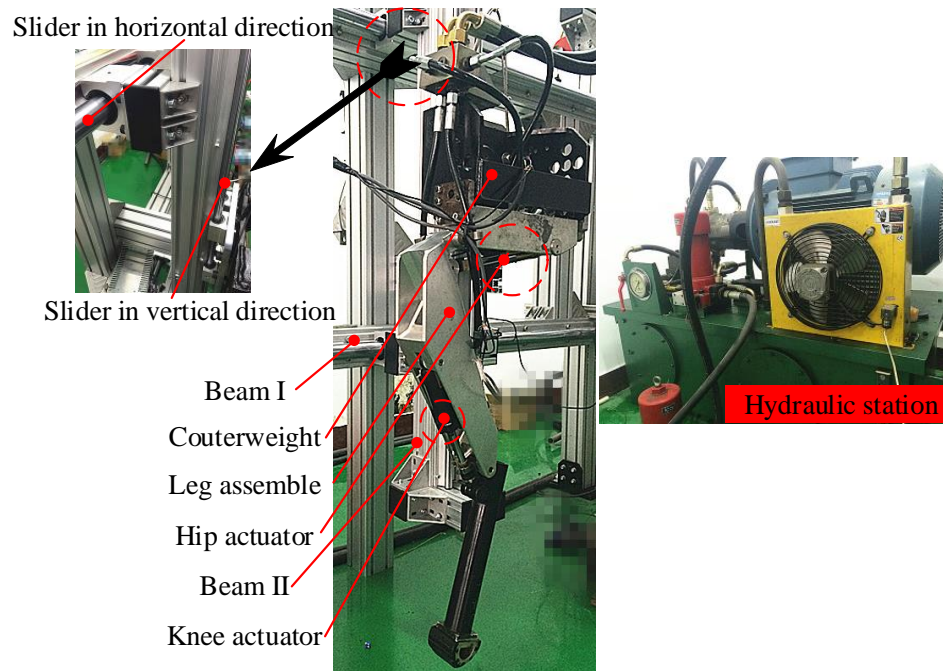


Figure 12. Test bench.

The stiffness and damping of the virtual model were set to 3500 N/m and 0 N/m/s on the  $x$ -axis and 5300 N/m and 0 N/m/s on the  $z$ -axis; the experimental process is shown in Figure 13. The accumulator models and the parameters used in the two groups are shown in Table 7.

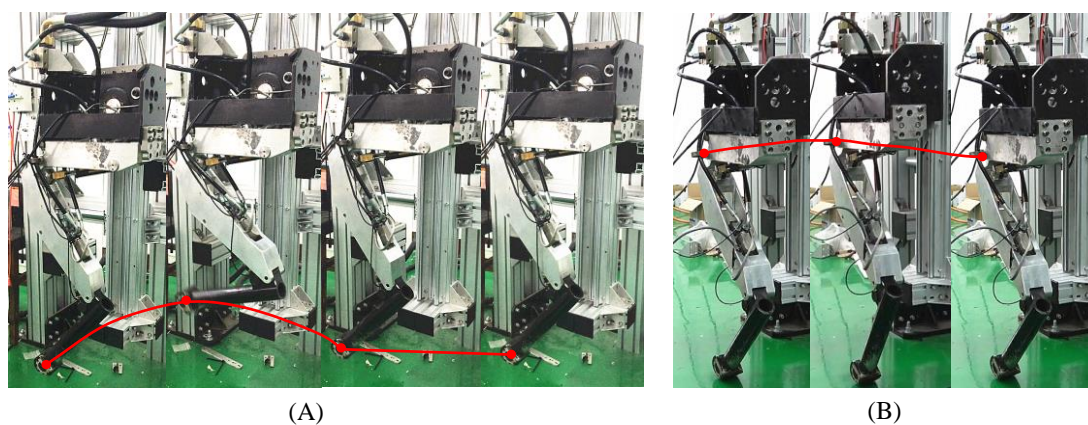


Figure 13. Trajectory tracing test. (A) Group 1; (B) group 2.

Table 7. Experimental grouping.

Case	Accumulator	Initial Pressure	Working Volume
different inflation pressure	HAWE AC-13-1/4	2 and 4 Mpa	$1.3 \times 10^{-5} \text{ m}^3$
different working volume	HAWE AC-13-1/4, AC-40-1/4	3 Mpa	$1.3 \times 10^{-5}$ and $4 \times 10^{-5} \text{ m}^3$

## 5.2. Experimental Results

The flow inter-conversion of the accumulator and piston chamber in group 1 is shown in Figure 14. The positive values indicate that the oil flows from the piston chamber to the accumulator, while negative values represent the opposite direction. It can be seen that, as the piston movement changes from extension to retraction, the accumulator undergoes a process of storing and releasing oil during each swing phase. In the swing phase, the extension of the piston accompanies the flow released, while the retraction of the piston accompanies the flow absorbed by the accumulator. In the supporting phase, all of the actuators are in the contraction stage. The reversing of the piston causes the pressure in the piston chamber to increase, and then part of the oil that should be expelled from of the actuators flows into the accumulator, so the values are negative. Due to errors of the sensor and calculation mode, there are little differences between the simulation and the experiment.

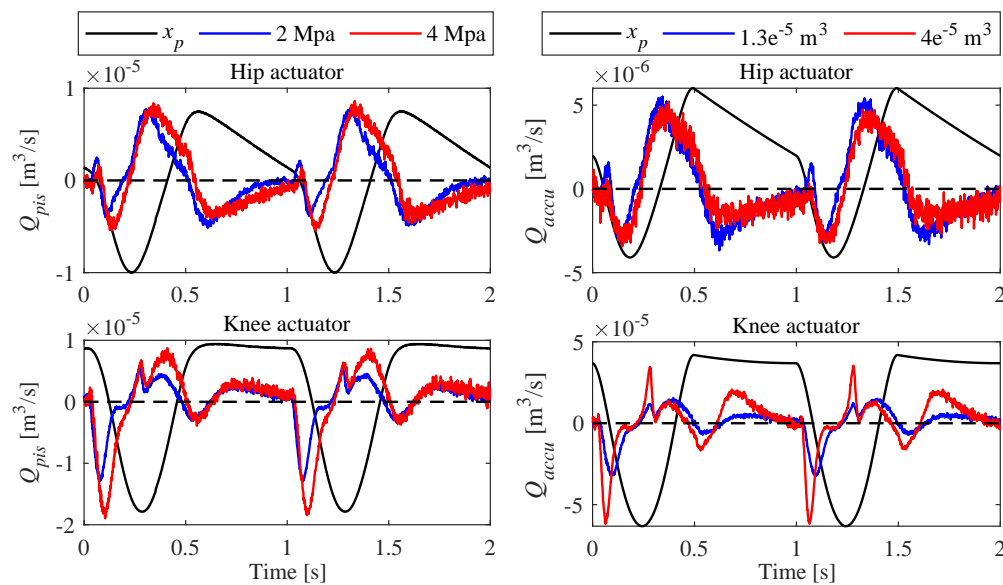


Figure 14. Flow of accumulator in group 1.

The energy consumption curves of the leg prototype in group 1 are shown in Figure 15. The energy consumption values of different conditions at time of two seconds are shown in Table 8. It can be seen from the data that the energy consumption of the leg prototype driven by HPCAs is reduced by more than 50 J compared to the original actuator.

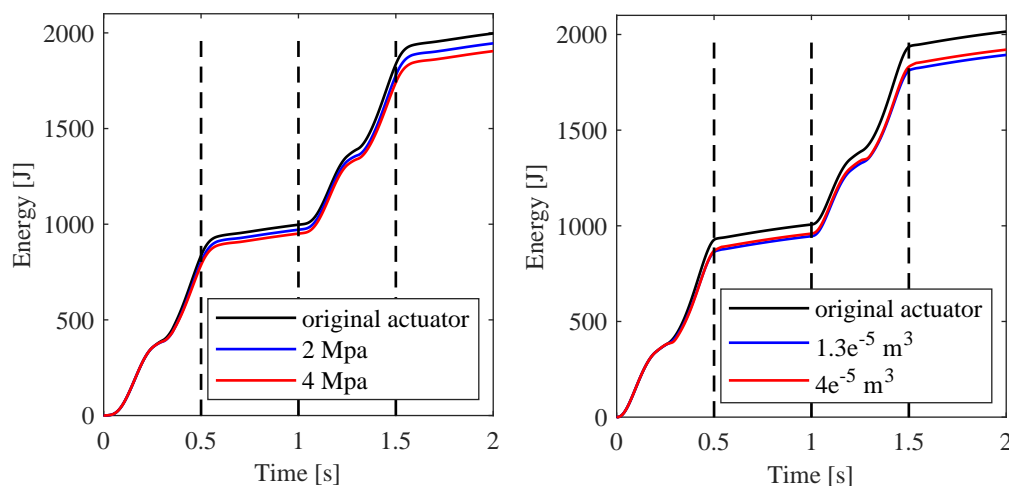
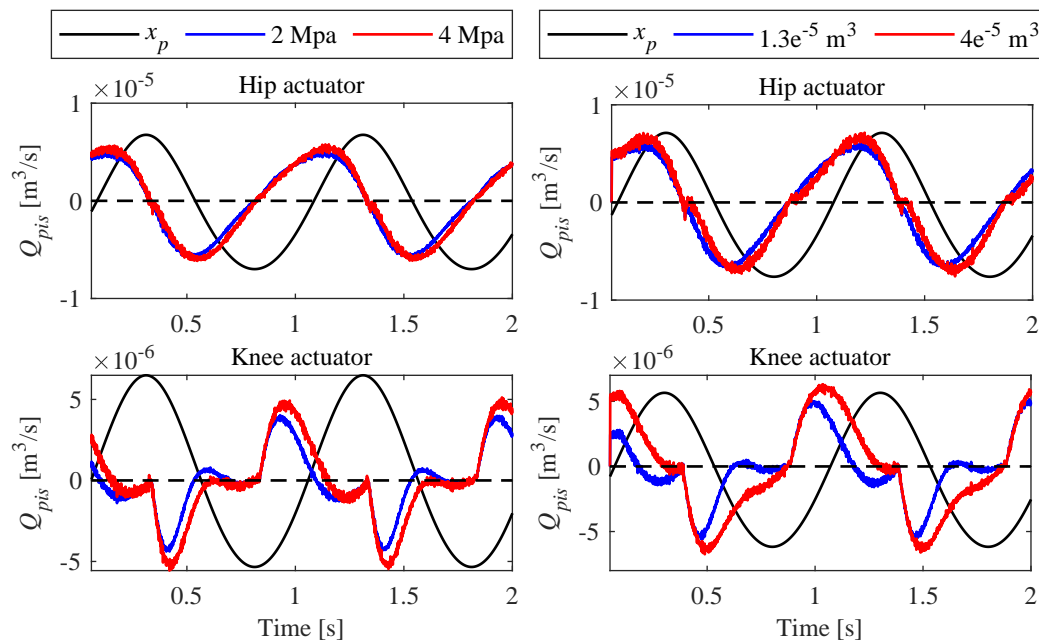


Figure 15. Energy consumption of leg prototype in group 1.

**Table 8.** Energy consumption of two gait cycle in group 1.

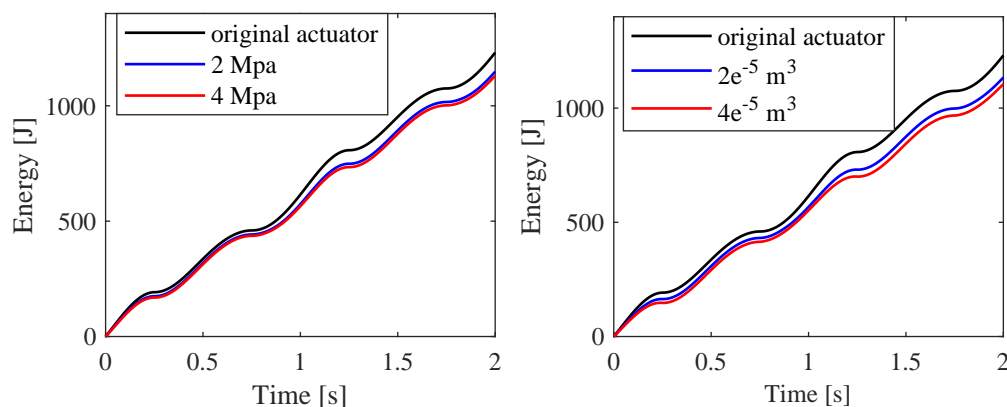
Description	Energy
original actuator	1997 J
2 Mpa	1945 J
4 Mpa	1915 J
$1.3 \times 10^{-5} \text{ m}^3$	1893 J
$4 \times 10^{-5} \text{ m}^3$	1921 J

Figure 16 shows the flow curves of group 2. It can be seen that the experimental results of group 2 are similar to those of group 1. The piston movement changes from extension to retraction, the accumulator undergoes a process of storing oil, and it undergoes a process of releasing oil when the reverse change takes place. According to the test results of the hip actuator, the changes in the initial inflation pressure and working volume of the accumulator have no obvious effect on the energy consumption of the HPCA, but for the HPCA that drives the knee F/E, the results are reverse. The main reason is that the knee actuator is subjected to a greater load than the hip joint due to the topology of the leg, and to a certain extent.

**Figure 16.** Flow of the accumulator in group 2.

The energy curves of the leg prototype in group 2 is shown in Figure 17. The energy consumption values of different conditions at time of two seconds are shown in Table 9. It can be seen from the data that the energy consumption of the leg prototype driven by HPCAs is reduced by more than 80 J compared to the original actuator.

From the above experiment results, it can be summarized that, although the initial inflation pressure or working volume of the accumulator does not have significant influence on the energy efficiency of the HPCA in the experiment, it is undeniable that the energy efficiency characteristics of the HPCA are also related to the load.



**Figure 17.** Energy consumption of leg prototype in group 2.

**Table 9.** Energy consumption of two gait cycle in group 2.

Description	Energy
original actuator	1231 J
2 Mpa	1148 J
4 Mpa	1130 J
$1.3 \times 10^{-5} \text{ m}^3$	1134 J
$4 \times 10^{-5} \text{ m}^3$	1105 J

## 6. Conclusions

The HPCA is a novel servo actuator for hydraulic quadruped robots to buffer the impact force between a robot's feet and the ground. First, by analyzing the static and dynamic pressure characteristics of the actuator and the motion law of the piston in the trotting gait, the efficiency characteristics of the HPCA are obtained. Then, a simulation analysis and the physical experiment are carried out to verify the energy-saving of the HPCA with different initial inflation pressures and working volumes. It can be demonstrated that the energy-saving performance of the HPCA depends on the pressure transition caused by the piston reversing. When the piston is moving from extension to retraction, part of oil that should flow out from the piston chamber is absorbed by the accumulator, while from retraction to extension, this part of the oil is released and used for piston movement. Moreover, for foot trajectories commonly used by quadruped robots with the same structure as SCalf, the HPCA has higher energy efficiency in the swing phase of the trotting gait compared to the hydraulic servo actuator with the original structure, and this characteristic does not change with the working volume and inflation pressure of the accumulator.

**Author Contributions:** Conceptualization, Z.H. and X.R.; software, Z.H. and Y.L.; writing, Z.H.; supervision, B.L.; funding acquisition, Y.L., X.R., S.Z. and H.C. All authors have read and agreed to the published version of the manuscript.

**Funding:** This work is supported by the National Natural Science Foundation of China [Grant No. U1613223, 61973185, 61703243], the National High Technology Research and Development Program of China [Grant No. 2017YFC0806505, 2015AA042201], the Development plan of Youth Innovation Team in Colleges and Universities of Shandong Province [2019KJN011].

**Conflicts of Interest:** The authors declare no conflict of interest.

## References

- Chen, T.; Rong, X.; Li, Y.; Ding, C.; Chai, H.; Zhou, L. A compliant control method for robust trot motion of hydraulic actuated quadruped robot. *Int. J. Adv. Robot. Syst.* **2018**, *15*. [\[CrossRef\]](#)
- Boaventura, T. Hydraulic Compliance Control of the Quadruped Robot HYQ. Ph.D. Thesis, Advanced Robotics Department, University of Genova, Genova, Italy, 2013.

3. Raibert, M.; Blankespoor, K.; Nelson, G.; Playter, R. BigDog, the Rough-Terrain Quadruped Robot. *IFAC Proc. Vol.* **2008**, *41*, 10822–10825. [[CrossRef](#)]
4. Wooden, D.; Malchano, M.; Blankespoor, K.; Howardy, A.; Rizzi, A.A.; Raibert, M. Autonomous navigation for bigdog. In Proceedings of the 2010 IEEE International Conference on Robotics and Automation, Anchorage, Alaska, 3–8 May 2010; pp. 4736–4741.
5. Nelson, G.; Saunders, A.; Playter, R. The petman and atlas robots at boston dynamics. In *Humanoid Robotics: A Reference*; Springer: Dordrecht, The Netherlands, 2019; pp. 169–186.
6. Seok, S.; Wang, A.; Chuah, M.Y.; Otten, D.; Lang, J.; Kim, S.; Wang, A.; Lang, J. Design principles for highly efficient quadrupeds and implementation on the MIT Cheetah robot. In Proceedings of the 2013 IEEE International Conference on Robotics and Automation, Karlsruhe, Germany, 6–10 May 2013; pp. 3307–3312.
7. Semini, C. HYQ-Design and Development of a Hydraulically Actuated Quadruped Robot. Ph.D. Thesis, University of Genoa, Genoa, Italy, 2010.
8. Bledt, G.; Powell, M.J.; Katz, B.; Di Carlo, J.; Wensing, P.M.; Kim, S. Mit cheetah 3: Design and control of a robust, dynamic quadruped robot. In Proceedings of the 2018 IEEE/RSJ International Conference on Intelligent Robots and Systems (IROS), Madrid, Spain, 1–5 October 2018; IEEE: Piscataway, NJ, USA, 2018; pp. 2245–2252.
9. Pratt, G.A.; Williamson, M.M. Series elastic actuators. In Proceedings of the 1995 IEEE/RSJ International Conference on Intelligent Robots and Systems: Human Robot Interaction and Cooperative Robots, Pittsburgh, PA, USA, 5–9 August 1995; Volume 1, pp. 399–406.
10. Hanafusa, H.; Asada, H. A robot hand with elastic fingers and its application to assembly process. In *Information-Control Problems in Manufacturing Technology*; Elsevier BV: Amsterdam, The Netherlands, 1978; pp. 127–138.
11. VanderBorgh, B.; Albu-Schaeffer, A.; Bicchi, A.; Burdet, E.; Caldwell, D.; Carloni, R.; Catalano, M.; Eiberger, O.; Friedl, W.; Ganesh, G.; et al. Variable impedance actuators: A review. *Robot. Auton. Syst.* **2013**, *61*, 1601–1614. [[CrossRef](#)]
12. Wolf, S.; Grioli, G.; Eiberger, O.; Friedl, W.; Grebenstein, M.; Höppner, H.; Burdet, E.; Caldwell, D.G.; Carloni, R.; Catalano, M.G.; et al. Variable stiffness actuators: Review on design and components. *IEEE/ASME Trans. Mechatron.* **2015**, *21*, 2418–2430. [[CrossRef](#)]
13. Hutter, M.; Gehring, C.; Lauber, A.; Gunther, F.; Bellicoso, C.D.; Tsounis, V.; Fankhauser, P.; Diethelm, R.; Bachmann, S.; Bloesch, M.; et al. ANYmal—Toward legged robots for harsh environments. *Adv. Robot.* **2017**, *31*, 918–931. [[CrossRef](#)]
14. Hutter, M.; Gehring, C.; Jud, D.; Lauber, A.; Bellicoso, C.D.; Tsounis, V.; Hwangbo, J.; Bodie, K.; Fankhauser, P.; Bloesch, M.; et al. ANYmal—A highly mobile and dynamic quadrupedal robot. In Proceedings of the 2016 IEEE/RSJ International Conference on Intelligent Robots and Systems (IROS), Daejeon, Korea, 9–14 October 2016; pp. 38–44.
15. Collins, S.H.; Wisse, M.; Ruina, A. A Three-Dimensional Passive-Dynamic Walking Robot with Two Legs and Knees. *Int. J. Robot. Res.* **2001**, *20*, 607–615. [[CrossRef](#)]
16. Tedrake, R.; Zhang, T.; Fong, M.-F.; Seung, H. Actuating a simple 3D passive dynamic walker. In Proceedings of the IEEE International Conference on Robotics and Automation, New Orleans, LA, USA, 26 April–1 May 2004; Volume 5, pp. 4656–4661.
17. Collins, S.H.; Ruina, A. A bipedal walking robot with efficient and human-like gait. In Proceedings of the 2005 IEEE International Conference on Robotics and Automation, Barcelona, Spain, 18–22 April 2005; pp. 1983–1988.
18. Kim, T.; So, B.; Kwon, O.; Park, S. The energy minimization algorithm using foot rotation for hydraulic actuated quadruped walking robot with redundancy. In Proceedings of the ISR 2010 (41st International Symposium on Robotics) and ROBOTIK 2010 (6th German Conference on Robotics), Munich, Germany, 7–9 June 2010; pp. 1–6.
19. Gebhardt, N. *Hydraulik: Grundlagen, Komponenten, Schaltungen*; Springer: Berlin, Germany, 2008.
20. Shenouda, A. Quasi-Static Hydraulic Control Systems and Energy Savings Potential Using Independent Metering Four-Valve Assembly Configuration. Ph.D. Thesis, Georgia Institute of Technology, Atlanta, GA, USA, 2006.



21. Liu, S.; Yao, B. *Energy-Saving Control of Single-Rod Hydraulic Cylinders with Programmable Valves and Improved Working Mode Selection*; SAE Technical Paper Series; SAE International: Warrendale, PA, USA, 2005; pp. 51–61. [[CrossRef](#)]
22. Jelali, M.; Kroll, A. *Hydraulic Servo-Systems: Modelling, Identification and Control*; Springer: London, UK, 2012.
23. Barasuol, V.; Villarreal-Magaña, O.A.; Sangiah, D.; Frigerio, M.; Baker, M.; Morgan, R.; Medrano-Cerda, G.A.; Caldwell, D.G.; Semini, C. Highly-Integrated Hydraulic Smart Actuators and Smart Manifolds for High-Bandwidth Force Control. *Front. Robot. AI* **2018**, *5*. [[CrossRef](#)]
24. Hua, Z.; Rong, X.; Li, Y.; Li, Y.; Sun, Y.; Su, B. Design, Modelling and Validation of Hydraulic Servo Actuator with Passive Compliance for Legged Robots. *IEEE Access* **2018**, *6*, 59486–59495. [[CrossRef](#)]
25. Rong, X. *Mechanism Design and Kinematics Analysis of a Hydraulically Actuated Quadruped Robot Scaff*; Shandong University: Jinan, China, 2013; Volume 10.
26. Hoyt, N.F.; Taylor, C.R. Gait and the energetics of locomotion in horses. *Nature* **1981**, *292*, 239–240. [[CrossRef](#)]
27. Hua, Z.; Rong, X.; Li, Y.; Chai, H.; Zhang, S. Active Compliance Control on the Hydraulic Quadruped Robot with Passive Compliant Servo Actuator. *IEEE Access* **2019**, *7*, 163449–163460. [[CrossRef](#)]
28. Niu, G.; Shang, F.; Krishnamurthy, M.; Garcia, J.M. Evaluation and selection of accumulator size in electric-hydraulic hybrid (EH2) powertrain. In Proceedings of the 2016 IEEE Transportation Electrification Conference and Expo (ITEC), Dearborn, MI, USA, 26–29 June 2016; pp. 1–6.
29. Merritt, H.; Merritt, H.E.; Merritt, H.E. *Hydraulic Control Systems*; John Wiley & Sons: Hoboken, NJ, USA, 1967.
30. Rydberg, K. Hydraulic accumulators as key components in energy efficient mobile systems. In Proceedings of the 6th International Conference on Fluid Power Transmission and Control, Huangzhou, China, 5–8 April 2005; pp. 124–129.
31. Lin, T.; Wang, Q. Hydraulic accumulator-motor-generator energy regeneration system for a hybrid hydraulic excavator. *Chin. J. Mech. Eng.* **2012**, *25*, 1121–1129. [[CrossRef](#)]
32. Marquis-Favre, W.; Bideaux, E.; Scavarda, S. A planar mechanical library in the AMESim simulation software. Part II: Library composition and illustrative example. *Simul. Model. Pr. Theory* **2006**, *14*, 95–111. [[CrossRef](#)]
33. Zapolsky, S.; Drumwright, E. Quadratic programming-based inverse dynamics control for legged robots with sticking and slipping frictional contacts. In Proceedings of the 2014 IEEE/RSJ International Conference on Intelligent Robots and Systems, Chicago, IL, USA, 14–18 September 2014; IEEE: Piscataway, NJ, USA, 2014; pp. 3266–3271.



© 2020 by the authors. Licensee MDPI, Basel, Switzerland. This article is an open access article distributed under the terms and conditions of the Creative Commons Attribution (CC BY) license (<http://creativecommons.org/licenses/by/4.0/>).